❏   559

Enhanced Three-Phase Inverter Fault Detection and Diagnosis Approach-Design and Experimental Evaluation

Hicham Fadil[1], Mohamed Larbi Elhafyani[2], Smail Zouggar[3]
Laboratory of Electrical Engineering and Maintenance (LGEM), Higher School of Technology,
University Med First Oujda, Morocco

Article Info	ABSTRACT
	Efficiency, reliability, high power quality and continuous operation are important aspects in electric vehicle attraction system. Therefore, quick fault detection, isolation and enhanced fault-tolerant control for open-switches faults in inverter driving systems become more and more required in this filed. However, fault detection and localization algorithms have been known to have many performance limitations due to speed variations such as wrong decision making of fault occurrence. Those weaknesses are investigated and solved in this paper using currents magnitudes fault indices, current direct component fault indices and a decision system. A simulation model and experimental setup are utilized to validate the proposed concept. Many simulation and experimental results are carried out to show the effectiveness of the proposed fault detection approach.

Corresponding Author:

Hicham Fadil,
Laboratory of Electrical Engineering and Maintenance (LGEM),
Higher School of Technology, University Med First Oujda.
BP 669, Oujda, 60000, Morocco
Email: hicham1fadil@gmail.com

1.   INTRODUCTION

Reliability and continuous operation at faulty cases have attracted the interest of many researches in the last decade [1], [2], [3]. Therefore, great interests haven been given to three-phase motor dive systems fault detection, localization and hardware/software reconfiguration [4]. These interests are justified since that the power inverter components were often identified as the weakest part of the dives system; Statistics studies [5], [6], [7] demonstrate that power semiconductors and gate drives failure rates are higher than other faults.

Given the security offered by the fault-tolerant topologies, they have been adopted in several applications such as in aerospace actuators [8], [9], in wheel motors [10], [11] and steer/brake by wire systems [12]. One of the most used power electronic topology is three-phase fault-tolerant power converter based on TRIACs as shown in Figure 1. It is exploited in electric vehicle permanent magnet synchronous machine (PMSM) drive system [13], in wind turbines [14] as will as in grid-side converter [15].

Numerous real-time algorithms have been proposed in literature with the interest of detecting and locating open switch faults. This localization has been performed in [16], [17] by current space vector trajectory diameter analyzing. Two methods based on the the $\alpha\beta$ currents are investigated in [18]; the current-vector trajectory and the derivative of the current-vector phase are analyzed. In [19], an artificial neural network has been trained by a faulty drive simulation model allowing to isolate the fault. In [20], the detection is based on the the $\alpha\beta$ currents analyzed by a fuzzy technique. additional voltage sensors are integrated in the dire topology in [21] to achieve fast detection and localization times using voltage-based techniques.

In this paper, an enhanced fault detection technique based on computing of the PMSM three-phase currents has been presented. The improved fault detection method is made up of three indices showing the modification of currents amplitudes, and three other indices showing PMSM currents average values.
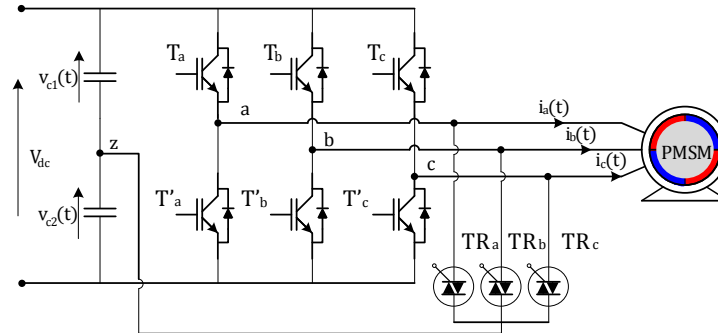

Figure 1. Fault tolerant power inverter topology

2.   INVERTER FEED PMSM MODEL AND CONTROL APROCHE

The three-phase six-switch inverter, shown in Figure 1, have been adopted to feed our three-phase closed-end winding permanent magnet synchronous machine. This topology was made under study because of its extensive uses in vehicle attraction field. To succeed the inverter continuous operation, each PMSM phase has been connected to the dc-capacitors mid-point through an additional TRIAC (*TRa*, *TRb* and *TRc*). These additional components are triggered once the algorithm, object of this article, discovers switch failure.

2.1. Permanent Magnet Synchronous Motor Model

Inverter switch fault detection and PMSM speed adjusting algorithms require the system model with an average complexity. Therefore, in what follows, we neglected the effects of flux saturation, saliency and the electromotive force (EMF) harmonic beyond the third harmonic component; controllers in speed/currents control loops tolerate several modelling simplifications, such as perfect sinusoidal distribution of stator winding. In addition, the produced magneto-motive-forces and the magnitude flux linkage through the stator winding are sinusoidal.

As a result, and adopting the (*abc*) rotating reference frame, the electrical model of the PMSM can be written as the following [22], [23]:

$$
\begin{aligned}
&\left[u_s(t)\right]^{abc} = R\left[i_s(t)\right]^{abc} + d\left[\psi_s(t)\right]^{abc}/dt \\
&\left[\psi_s(t)\right]^{abc} = \begin{bmatrix} L & M & M \\ M & L & M \\ M & M & L \end{bmatrix}\left[i_s(t)\right]^{abc} + \Psi_m \begin{bmatrix} \cos(\theta_r) \\ \cos(\theta_r - 2\pi/3) \\ \cos(\theta_r + 2\pi/3) \end{bmatrix}.
\end{aligned}
\tag{1}
$$

Where $\left[u_s(t)\right]^{abc}$, $\left[i_s(t)\right]^{abc}$ and $\left[\psi_s(t)\right]^{abc}$ are the stator voltage, current and flux vectors, *L* and *M* are the stator winding self-inductance and the mutual-inductance between the windings, Ψ_m is the maximal amplitude of the permanent magnet flux and θ_r is the electrical rotor position.

In order to simplify modelling, given that the investigated synchronous motor in this paper is a surface mounted permanent magnet motive, the stator winding inductances L and M are adopted constants. Consequently, the notation $L_s = L - M$ can be made.

By adopting the aforementioned assumptions, a PMSM mechanical model can be formulated as:

$$
J\frac{d}{dt}\Omega = T_{em} - f_r\Omega - T_{Load}
\tag{2}
$$

To achieve the vector control, and to make speed adjusting and controllers sizing easy, Park transformations from/to the rotating reference frame linked to the rotor are required. By applying Park

transforms presented in [20] to Equations (1) and (2), the state-space equations of the dynamic electrical and mechanical systems can be obtained:

$$\frac{d}{dt}\begin{bmatrix} i_d \\ i_q \\ \Omega \end{bmatrix} = \begin{bmatrix} -R/L_s & P\Omega & 0 \\ -P\Omega & -R/L_s & -P\Psi_m/L_s \\ 0 & 3P\Psi_m/2J & -f_r/J \end{bmatrix} . \begin{bmatrix} i_d \\ i_q \\ \Omega \end{bmatrix} + \begin{bmatrix} 1/L_c & 0 & 0 \\ 0 & 1/L_c & 0 \\ 0 & 0 & 1/J \end{bmatrix} . \begin{bmatrix} u_d \\ u_q \\ T_{Load} \end{bmatrix}$$

$$[\Omega] = \begin{bmatrix} 0 & 0 & 1 \end{bmatrix} . \begin{bmatrix} i_d \\ i_q \\ \Omega \end{bmatrix}$$

$$(3)$$

Where u_d, u_q are the stator d- and q-axes voltages, i_d, i_q are the stator d- and q-axes currents, R is the stator resistance, Ω is the rotor angular velocity, P is pairs pole number, T_{load} is the load torque, fr is the viscous friction coefficient and J is the inertia moment.

The created torque in PMSMs at the healthy operation mode is smooth due to the interaction between the three balanced sinusoidal stator current and rotor flux, and it can be described by:

$$T_{em} = 3P\Psi_m i_q/2 \tag{4}$$

It is noticed from the equation (3) that the model in the rotating reference frame is coupled, and it contains nonlinear terms. Then, to achieve the vector control, the opted control loop, must be consisting of a decoupling block, a model linearization and additionally two control loops [22]-[23]-[28].

2.2. Inverter Model

In order to simplify inverter modelling, The IGBT are stimulated by an ideal switches with no died band time throughout this paper as it assumed in [24]-[25]. Consequently, the switches can be denoted by Boolean variables S_x, $S_x^{'}$ (x=a, b or c). Therefore, the binary values '1' of each switch   will indicate the closed state of them. Whereas, the binary values '0' will indicate the opened state. Based on that assumption, the created three-phase voltages using the source neural point are given as follows:

$$V_{xn} = \begin{cases} V_{dc}/2 \text{ si } S_x = 1 \\ -V_{dc}/2 \text{ si } S_x^{'} = 1 \end{cases} \tag{5}$$

Where 'n' is a fictitious neutral point used to simplify the modeling and the voltage computation, and V_{dc} is the voltage supplying the inverter. The equation 6 is no longer validated in case of transistors failure of the inverter, and the resulting voltage depend on the fault type. The three types of faults, which can be occur in one leg in addition to the healthy operation, are presented in Figure 2.

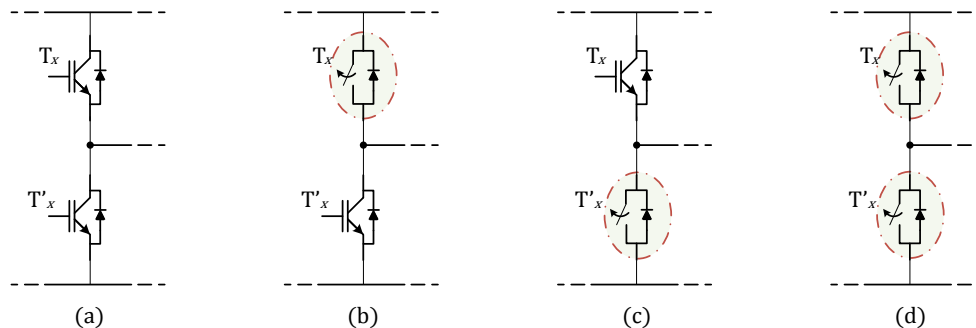|			
(a)	(b)	(c)	(d)

Figure 2. One leg faults types: (a) healthy leg; (b) Fault of the upper switch; (c) Fault of the lower switch; (d) Fault of one leg

In case of one leg fault (Open fault of two switches), the linked phase current becomes equal to zero. Consequently, and from the equation 5, the voltage at the terminals of the corresponding coil equal to the EMF produced by the permanent magnet rotation. In case of one switch failure (one Open fault of switch), the generated voltage depends on the faulty switch. Moreover, the equation 5 could be rewritten for each fault. For example, when the switch 'S_x' is in fault, it is no longer possible to apply $V_x = V_{dc}/2$. However, since the free-wheeling diode is in good condition, the generated voltage is as follows:

If $I_x < 0$ the same generated voltage as it in the equation 5.

If $I_x \geq 0$ the same generated voltage is presented in the equation 6.

$$V_{xn} = \begin{cases} -V_{dc}/2 \ if \ S_x = 1 \\ -V_{dc}/2 \ if \ S_x' = 1 \end{cases} \tag{6}$$

As a result, the faulty leg could not apply positive voltages, as well as positive current. This current waveform reduces torque quality and increases its total harmonic distortion (THD) value.

3.   FAULT DITECTION INDECES

From the previous section, where the system behaviors under faulty component was analyzed, it can be concluded that any switch failure affects the associated phase current; the magnitude of the fundamental harmonic of the current is lower, and a direct current component is added. These current changes are the indicators that allow localizing the fault component without additional sensors.

In what follows, a quadrature-signal generator is introduced to extract the fundamental harmonic of currents and their magnitude. Moreover, an adapting low-pass filter is sized to extract direct current component. Based on these quantities, fault indices are computed and decision system is made.

3.1. Phase Currents Magnitude Computing

The implemented filter structure, shown in Figure 3, has been widely used for many years [26]-[27], it consists of an adaptive resonant filter capable of filtering the fundamental harmonic of currents from an input current, and generating its quadratic. To make this filter bandwidth adaptable, the resonance frequency is returned external and computed from the PMSM speed.
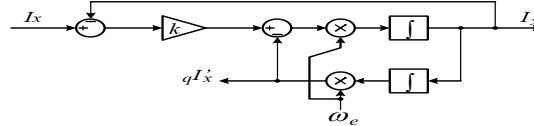

Figure 3. Quadratic signal generator (QSG)

$$D(s) = \frac{I_x'}{I_x}(s) = \frac{k\,\omega_e s}{s^2 + k\,\omega_e s + \omega_e^2} \tag{7}$$

$$Q(s) = \frac{qI_x'}{I_x}(s) = \frac{k\,\omega_e}{s^2 + k\,\omega_e s + \omega_e^2} \tag{8}$$

The transfer functions between the filter inputs and the generated signals (I'_x and qI'_x) are defined by the equations 7 and 8. And It can be noticed that the filter bandwidths are linked to the gain k and to the PMSM electrical frequency ω_e. Given that, the filter generates a pure sinusoidal current and its quadratic quantities, current magnitude M_x for each phase could be obtained by calculating:

$$M_x = \sqrt{(I_x')^2 + (qI_x')^2} \tag{9}$$

Where I_x' is the x phase current fundamental and qI_x' is the quadratic component of the same phase current.

3.2. Filtering the Phase currents Mean Value

In case of one open-switch fault occurrence, the current of the associated phase is shifted, and a direct current is added. This current quantity value leads to identify the faulty switch. Consequently, the used low-pass filter (LPF), shown in figure 4, have ben modified, and its bandwidth become adjustable to track speed variation. Its transfer function is presented by the equation 10.
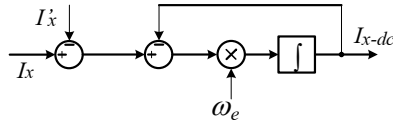
$$\frac{I_{x-dc}}{I_x - I_x'}(s) = \frac{\omega_e}{s + \omega_e} \qquad (10)$$

Figure 4. Low-pass current filter with an adapting bandwidth

One can notice, that the fundamental component is subtracted from the current before the filtering which have been done in order minimize the filtered low frequencies harmonics.

3.3. Indices Computing

Appropriate fault indices are gotten if the following rules are achieved:

a. the indices values must be close to zero in healthy operation and large in case of fault;
b. the indices values in case of fault must allow these faults isolation;
c. the indices must not be insensitive to the operating conditions (speed and load)

Using phase-currents magnitudes and their mean values, the following indices are recommended

$$R_{M_{ab}} = \left| \frac{M_a - M_b}{\max(M_a, M_b, M_b)} \right|$$

$$R_{M_{bc}} = \left| \frac{M_b - M_c}{\max(M_a, M_b, M_b)} \right| \qquad (11)$$

$$R_{M_{ca}} = \left| \frac{M_c - M_a}{\max(M_a, M_b, M_b)} \right|$$

$$R_{DC_a} = \frac{I_{a-dc}}{\max(M_a, M_b, M_c)}$$

$$R_{DC_b} = \frac{I_{b-dc}}{\max(M_a, M_b, M_c)} \qquad (12)$$

$$R_{DC_c} = \frac{I_{c-dc}}{\max(M_a, M_b, M_c)}$$

3.4. Decision system

The decision system objectives are to analyze the fault indices in order to locate the faulty switches and make the decision to adjust the power electronic in order to isolate the faulty leg.

Since the fault indices, calculated by equations 11 and 11, are variables and change along healthy and faulty operation. For this reason, the flowcharts presented below is adopted to produce the instructions for the decision system.
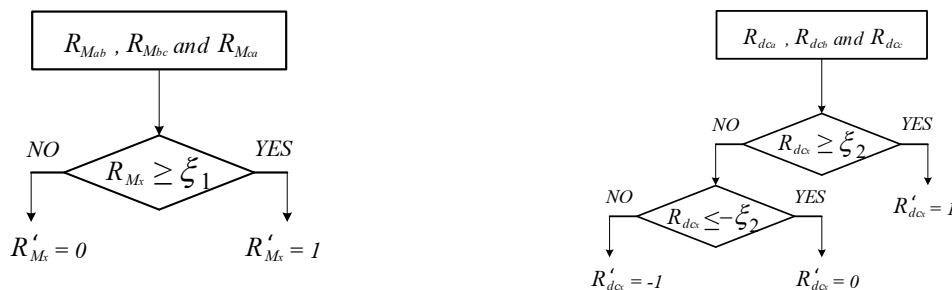

Figure 5. Magnitude and direct current fault indices flowcharts

In those flowcharts, the magnitude fault indices variation are divided into two intervals; if $R_{M_x} \geq \zeta_1$ then the new index R'_{M_x} is equal 1, else, it is equal to 0. However, the direct current fault indices variation are divided into three intervals variations; if $R_{dc_x} \geq \zeta_2$ then the new index R'_{DC_x} is equal one, if $R_{dc_x} \leq -\zeta_2$ it is equal to -1, else, it is equal to 0.

From the revealed intervals classification, and using table 1 of the decision logic, the determination of the faulty phase or even the faulty transistor has become feasible. To define the intervals limits ζ_1 and ζ_2, intensive tests are carried out in the following section.

Table 1. Localization Chart of Faulty Components Location

Transistor Ouvert	T_a	T_b	T_c	T'_a	T'_b	T'_c	$T_a \& T'_a$	$T_b \& T'_b$	$T_c \& T'_c$
$R'_{M_{ab}}$	1	1	0	1	1	0	1	1	0
$R'_{M_{bc}}$	0	1	1	0	1	1	0	1	1
$R'_{M_{ca}}$	1	0	1	1	0	1	1	0	1
R'_{DC_a}	-1	x	x	1	x	x	0	x	x
R'_{DC_b}	x	-1	x	x	1	x	x	0	x
R'_{DC_c}	x	x	-1	x	x	1	x	x	0

4. INVERTER FEED PMSM MODEL AND CONTROL APROCHE

The proposed fault detection Indices, presented previously, and the power configuration were tested in simulation; the power structure was assembled in PSIM which had been interconnected to Matlab/Simulink. In addition, the control scheme and the faults detection systems were built in Simulink. The validated algorithm was then implemented by means of the test bench shown in Figure 6.
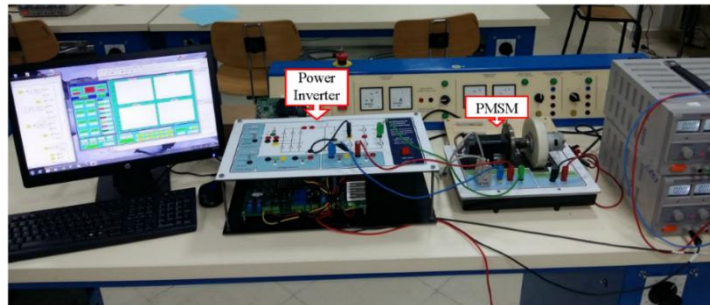

Figure 6. Experimental setup including eZdsp , PMSM and power inverter

A 32-bit floating-point TMS320-F28335 digital signal processor (DSP) board, based on a 150 MHz clock, accomplished the drive system; it has been programed using Matlab/Simulink® rapid prototyping tools. A Matlab/GUI real time interface locally built was used to make results recording easy [28]. The power structure includes a six-switch three-phase inverter associated to split capacitors. The 6S3P inverter is feeding a PMSM with Surface Magnet Mounted. Parameters and other configuration requirements are presented in table 2. To operate around nominal point, the PMSM was loaded by DC generator supplied by a current source to establish a fixed load torque. An incremental encoder was used to measure rotor position (2000 pulse per revolution). These equipment, are illustrated in Figure.

Table 2. Inverter, Controller and PMSM Parameters

Components	Values	Components	Values
DC-voltage	24 V	Rated Power and Speed	P=80W, Ω=4000 rpm
PWM frequency	FPWM=12kHz	Pole pairs	4
Sampling	fs=10kHz	Viscous friction	fr = 0.04 10^{-3} Kgm^2
Upper/Lower capacitor C_1/C_2	4400μF	Rotation inertia	J = 0.5 10^{-3} Nm/rad
Inverter rated power	1kW	Resistance and inductance	R=0.43Ω, L=1.35 mH

To analyze the current behaviors, the three significant operations (healthy operation, operation with the upper open-switch fault and with one leg open-switches fault in phase 'c') have been tested in simulation and confirmed experimentally in order to validate the implemented model. Those tests are accomplished at constant speed $\Omega = 500$ rpm and with 60% of nominal load (0,09Nm). The obtained results are shown in figures 7, 8 and 9. Plots in figures 7a and 7b at healthy operation demonstrate that the generated currents are balanced and similar. On the other hand, plots in figures 8a and 8b with the upper open-switch fault in phase 'c' operation clearly show that the faulty phase current is distorted; the faulty phase current has taken only negative values. This behavior is due to the inverter, which cannot generates a voltage greater than the EMF when the faulty phase current in positive. However, for the other half period, when the phase 'c' current is negative, the inverter operates as a healthy one for the reason that the faulty switch purposes are accomplished by the associated freewheel diode. It can be concluded from results in figure 9, obtained through simulation and through experiment for one leg open-switches fault in phase 'c', that both behaviors are very similar, and extra harmonic currents are appeared in experimental results. In addition to that, one can observe that currents in both cases have become higher to compensate the lost 30% of torque.

Figure 10 shows the torque experimental results at 500 rpm when the machine is under 60% of nominal load. The top row figures show the torque behavior results in the three operation conditions previously mentioned. However, to quantify the generated torque distortion at 500 rpm, an FFT analysis using the Simulink tool with the fundamental harmonic of 33.33 Hz is done, and the results are shown in the bottom row figures. One can observe from results figure 10b obtained by operating with one open-switch that a first, second, and third harmonics have been added and the THD becomes equal to 58,56% against 8,7% at healthy operation. Moreover, when one leg open-switches fault is applied, THD is raised to 73,33%. Given that the torque ripple becomes higher in faulty cases, quick localization and rejection are highly required.
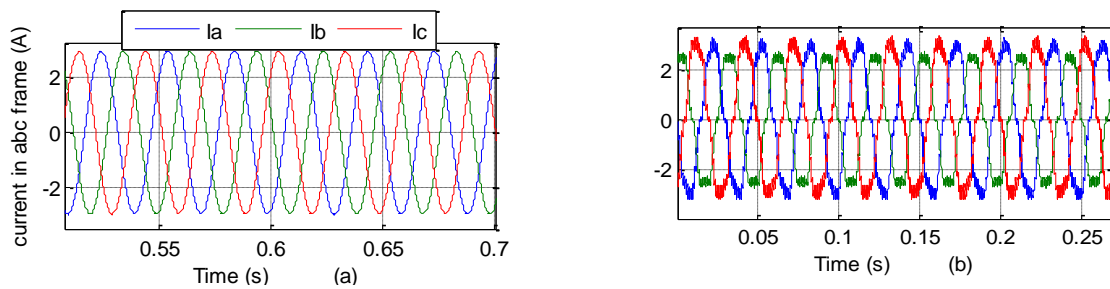

Figure 7. Three-phase motor current Ia, Ib and Ic, in healthy operation with $\Omega = 500$ rpm and Iq = 3 A; (a) simulation result; (b) experimental result
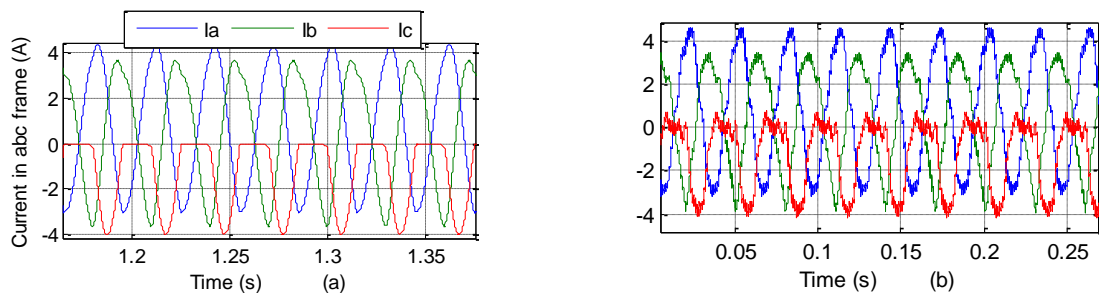

Figure 8. Three-phase motor current I_a, I_b and I_c, in operation with the upper open-switch fault in phase 'c' with $\Omega = 500$ rpm and $I_q = 3$ A; (a) simulation result; (b) experimental result
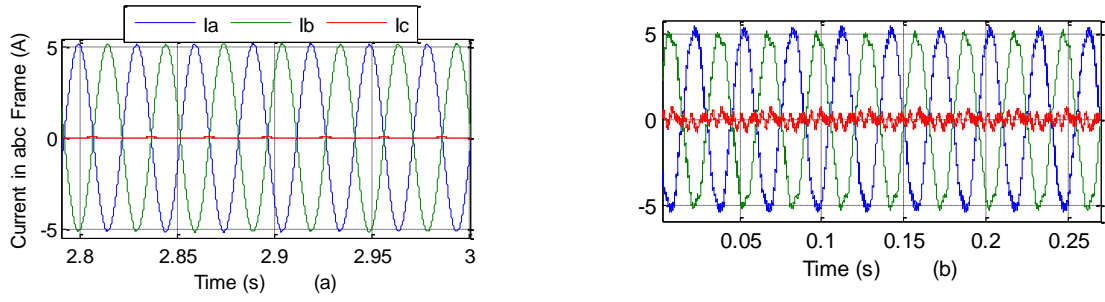
Figure 9. Three-phase motor current I_a, I_b and I_c, in operation with one leg open-switches fault in phase 'c' with Ω=500 rpm and $I_q = 3$ A; (a) simulation result; (b) experimental result
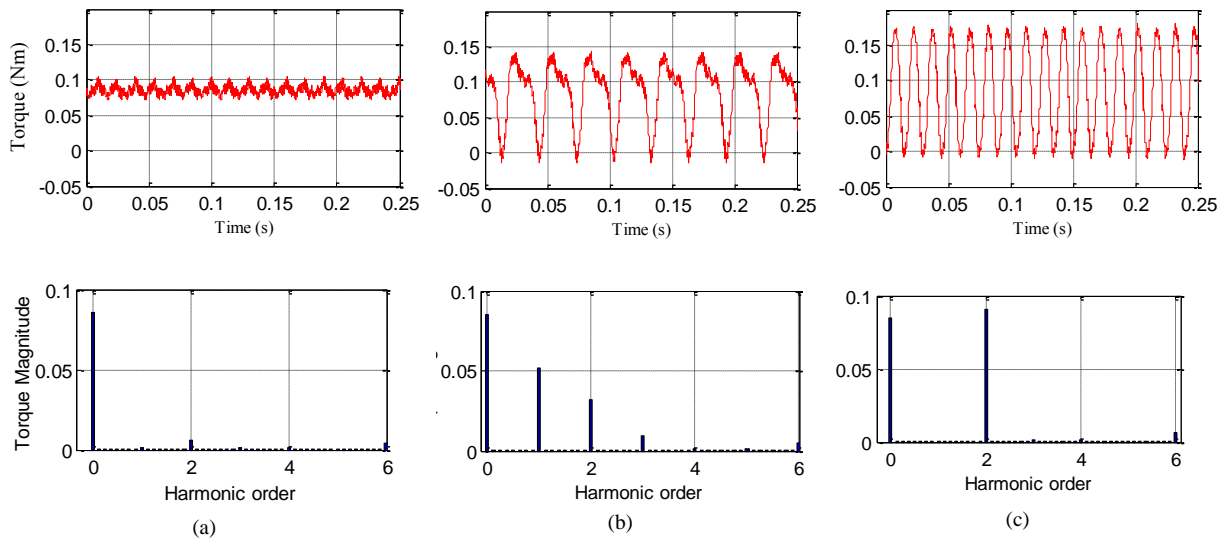

Figure 10. Experimental waveforms of the motor torque and their frequency analyses under three faults types; (a) in healthy operation; (b) with the upper open-switch fault; (c) with one leg open-switches fault
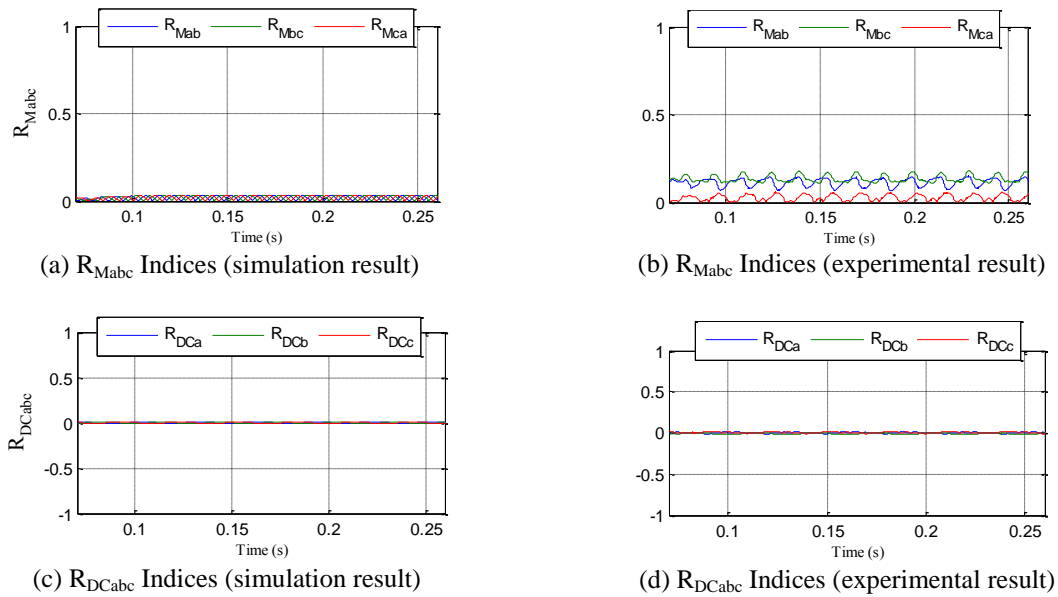

(a) R_{Mabc} Indices (simulation result)

(b) R_{Mabc} Indices (experimental result)

(c) R_{DCabc} Indices (simulation result)

(d) R_{DCabc} Indices (experimental result)

Figure 11. Fault indices behaviors in simulation and in experiment in healthy operation with $\Omega = 500$ rpm and I_q=3 A;

The simulation and experimental results of magnitude fault indices calculated in equation 11 and of mean value fault indices in equation 12, performed at healthy operation and presented in figures 11, conform that we have a good concordance between them, and those indices are close to zero when the PMSM currents are balanced (in this faultless case). Although, slight oscillations and offsets are appeared in experiment due to PMSM magnetic circuit and of Hall effect sensors.

Figure 12 demonstrates that the fault indices, in operation with the upper open-switch fault, are strongly affected, i.e. $R_{M_{bc}}$, $R_{M_{ca}}$ and R_{dc_c} .All of those indices are associated to the faulty phase.
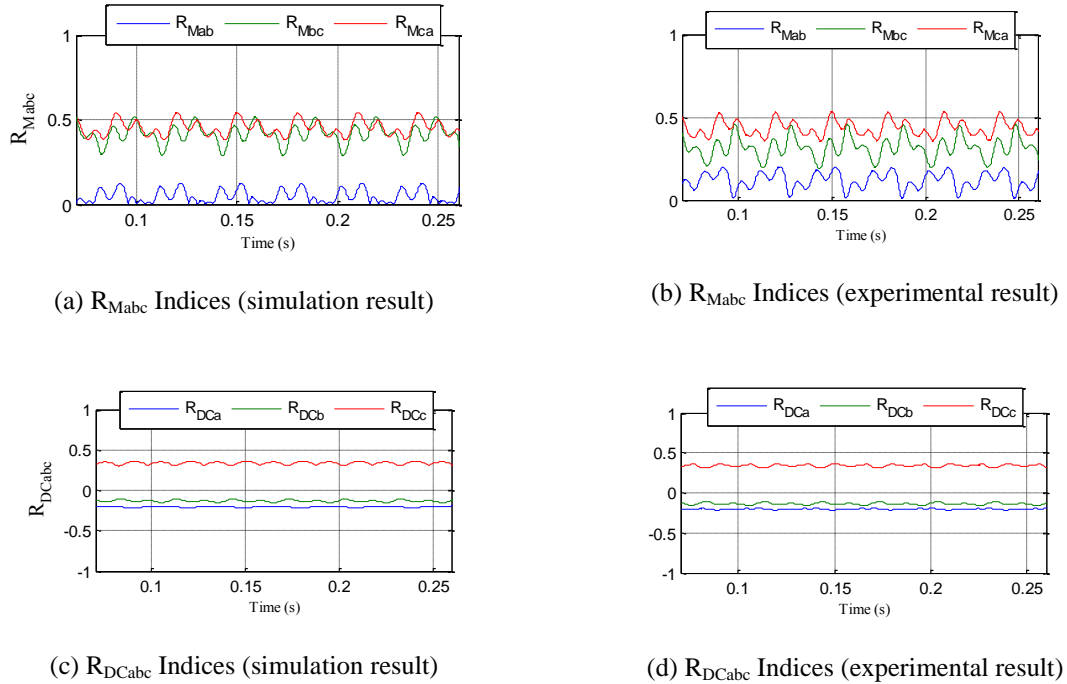

(a) R$_{Mabc}$ Indices (simulation result)

(b) R$_{Mabc}$ Indices (experimental result)

(c) R$_{DCabc}$ Indices (simulation result)

(d) R$_{DCabc}$ Indices (experimental result)

Figure 12. Fault indices behaviors in simulation and in experiment in operation with the upper open-switch fault in phase 'c' with Ω = 500 rpm and I_q = 3 A

(a) R$_{Mabc}$ Indices (simulation result)

(b) R$_{Mabc}$ Indices (experimental result)

(c) R$_{DCabc}$ Indices (simulation result)
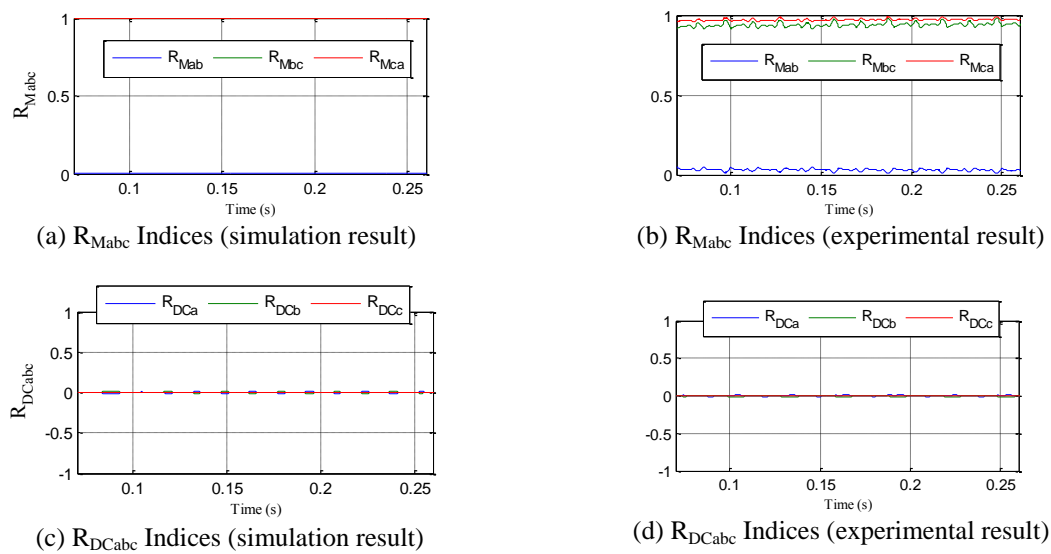
(d) R$_{DCabc}$ Indices (experimental result)

Figure 13. Fault indices behaviors in simulation and in experiment in operation with one leg open-switches fault in phase 'c' with Ω = 500 rpm and I_q = 3 A

When one open-switch fault is occurred in an inverter leg, tow operation states are possible; in the first half period, the system works as a healthy one, and the second half period, the system works as a faulty one. As a result, the magnitude fault indices alternate between large and low values. Moreover, the mean value fault indices become different from zero. It can also be detected from figures 12a and 12b that the minimum values of $R_{M_{bc}}$ and $R_{M_{ca}}$, in simulation and experimentally, are slightly differ and are lower in the experiments. While the maximum value of non-concerned index $R_{M_{ab}}$ are higher in the experiments. These issues make difficult the purpose of thresholds, and make necessary the accomplishment intensive testing on whole PMSM operation speed range.

Figure 13 shows fault indices behaviors in simulation and in experiment in operation with one leg open-switches fault in phase 'c'. One can observe that the magnitude fault indices $R_{M_{bc}}$ and $R_{M_{ca}}$, which are linked to the faulty phase, are highly affected. However, the direct current fault indices R_{DCabc} remains unchanged by default.

In order to implement the flowcharts presented in figure 5, and to make the faulty components localization possible table 1, the fault indices thresholds have been defined by applying a variable reference speed on the machine in the four operating cases, and observing the fault indices behavior.
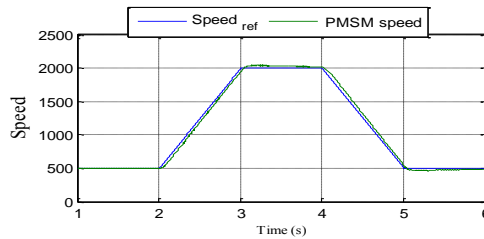

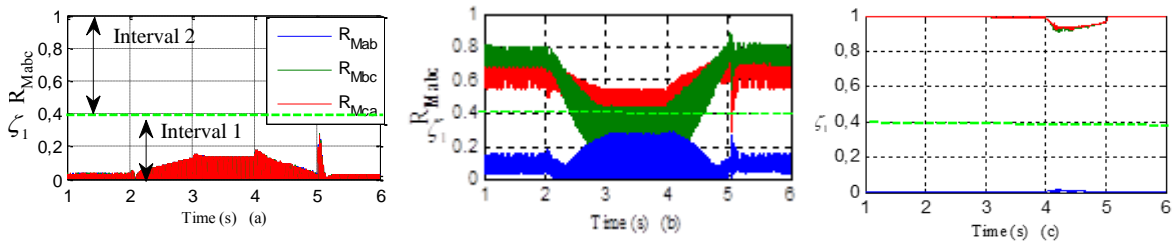Figure 14. Speed variation from 500 to 2000 rpm

Figure 15. R_{Mabc} fault indices behaviors in case of speed variation from 500 to 200 rpm and $I_q = 3$ A; (a) in healthy operation; (b) with the upper open-switch fault; (c) with one leg open-switches fault
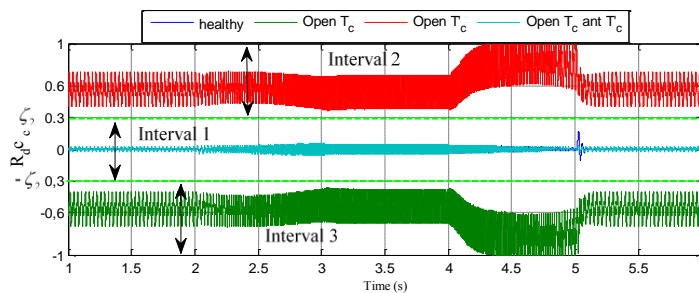

Figure 16. R_{DCc} fault index behaviors at the trees fault types operations and at healthy operation in case of speed variation from 500 to 200 rpm and $I_q = 3$ A

Figure 14 presents the speed tracking capability and reliability. Indeed, starting from a steady state at 500 rpm, 2000 rpm acceleration and deceleration profiles were applied respectively at $t = 2$ s and $t = 5$ s. The obtained results show that the speed profile tracking was slightly affected in the faulty operations.

It can be concluded form the magnitude fault indices behavior, in the four cases presented in figure 15, that the R_{Mx} linked to the faulty leg are higher than $\zeta_1 = 0.4$. On other hand, the direct current fault index linked to the faulty leg, presented in figure 16, varies above $\zeta_2 = 0.3$ when the lower switch is under fault, under $-\zeta_2 = -0.3$ when the upper switch is under fault and finally between ζ_2 and $-\zeta_2$ at the healthy operation case and at one leg open-switches fault.

5.   CONCLUSION

The important feature required in electrical attraction system is reliability; it is ensured by adding fault tolerance topology to maintain the continuity of operation, reject torque ripple and system break down under a variety of inverter faulty conditions. Indeed, the experimental torque results demonstrate that the torque ripples increase considerably at the faulty cases. In this work, the quickness and accuracy of open-switches fault tolerance topology are ensured with development of fault detection method based on the PMSM three-phase currents magnitudes and mean values. Two indices types are revealed (currents magnitudes and direct components fault indices) and computed under four possible operation condition (in healthy operation, with the upper/lower open-switch fault and with one leg open-switches fault).

The effectiveness of the proposed fault localization indices are strongly tested through a series of simulation and experimental tests. The results demonstrate that the generated indices, associated to the faulty leg, are highly affected and the indices associated to the other legs are perturbed as well. Furthermore, two thresholds are defined to separate indices values signification, and to make the faulty switches localization easy.

REFERENCES

[1]   T. M. Jahns, "Improved Reliability in Solid-State AC Drives by Means of Multiple Independent Phase Drive Units," *IEEE Transactions on Industry Applications*, vol. 16, no. 3, pp. 321-331, May 1980.

[2]   D. Venkata Ramana, S. Baskar, " Incipient Fault Detection of the Inverter Fed Induction Motor Drive, " *International Journal of Power Electronics and Drive System,* vol. 8, no. 2, pp. 722 - 729, June 2017.

[3]   B. Boudjellal, T. Benslimane, "Open-switch Fault-tolerant Control of Power Converters in a Grid-connected Photovoltaic System, " *International Journal of Power Electronics and Drive System,* vol. 7, no. 4, pp. 1294-1308, December 2016.

[4]   Y.-seok Jeong, S. K. Sul, S. E. Schulz, and N. R. Patel, "Fault detection and fault-tolerant control of interior permanent-magnet motor drive system for electric vehicle," *IEEE Transactions on Industry Applications*, vol. 41, no. 1, pp. 46–51, 2005.

[5]   S**.** Yang, A. Bryant, P. Mawby, D. Xiang, L. Ran and P. Tavner, "An industry-based survey of reliability in power electronic converters," *IEEE Transactions on Industry Applications*, vol. 47, no. 3, pp. 1441-1451, May-June 2011.

[6]   M. F. Habban, M. Manap, A. R. Abdullah, M. H. Jopri, T. Sutikno, " An Evaluation of Linear Time Frequency Distribution Analysis for VSI Switch Faults Identification, " *International Journal of Power Electronics and Drive System,* vol. 8, no. 1, pp. 1 - 9, March 2017.

[7]   K. Varalakshmi, R.L. Narasimham, G. Tulasi Ramdas, "Eccentric operation of STATCOM Using Predictive Controller, " *International Journal of Power Electronics and Drive System,* vol. 9, no. 1, pp. 150 - 156, March 2017.

[8]   O. Wallmark, L. Harnefors and O. Carlson, "Post-fault operation of fault-tolerant inverters for PMSM drives," *European Conference on Power Electronics and Applications*, 10 pp., 2005.

[9]   D. U. C. Delgado, D. R E. Trejo and E. Palacios, "Fault-tolerant control in variable speed drives: a survey," *IET Electric Power Applications*, vol. 2, no. 2, pp. 121-134, March 2008.

[10]   S. Bolognani, M. Zordan and M. Zigliotto, "Experimental fault-tolerant control of a PMSM drive," *IEEE Transactions on Industrial Electronics*, vol. 47, no. 5, pp. 1134-1141, October 2000.

[11]   N. Bianchi, S. Bolognani, M. Zigliotto, M. Zordan, "Innovative remedial strategies for inverter faults in IPM synchronous motor drives, "*IEEE Transactions on Energy Conversion*, vol. 18, no. 2, pp. 306- 314, June 2003.

[12]   K. D. Hoang, Z. Q. Zhu, M. P. Foster and D. A. Stone, "Comparative study of current vector control performance of alternate fault tolerant inverter topologies for three-phase PM brushless ac machine with one phase open-circuit fault," *In 5th IET International Conference on Power Electronics, Machines and Drives*, April 2010, pp. 19-21.

[13]   J. O. Estima, A. J. M. Cardoso, "Fast fault detection isolation and reconfiguration in fault-tolerant permanent magnet synchronous motor drives," *in Proc. IEEE Energy Convers. Congr. Expo.* 2012, pp. 3617-3624.

[14]   N. M. A. Freire, J. O. Estima, J. António and C. Marques, "A New Approach for Current Sensor Fault Diagnosis in PMSG Drives for Wind Energy Conversion Systems," *IEEE Transactions On Industry Applications*, vol. 50, no. 2, pp. 1206-1214, March/April 2014.

[15] N. A. Freire and A. J. Cardso, "A fault-tolerant direct controlled PMSG drive for wind energy conversion systems," *IEEE Trans. Ind. Electron.*, vol. 61, no. 2, pp. 821-834, Feb. 2014.

[16] R. Peuget, S. Courtine and J. P. Rognon, "Fault detection and isolation on a PWM inverter by knowledge-based model," *IEEE Transactions on Industry Applications*, vol. 34, no. 6, pp. 1318–1326, Nov./Dec., 1998.

[17] M. Trabelsi, M. Boussak and M. Gossa, "Multiple IGBTs open circuit faults diagnosis in voltage source inverter fed induction motor using modified slope method," *In XIX International Conference on Electrical Machines*, 2010, pp., 6-8.

[18] R. Peuget, S. Courtine and J. P. Rognon, "Fault detection and isolation on a PWM inverter by knowledge-based model," *IEEE Transactions on Industry Applications*, vol. 34, no. 6, pp. 1318–1326, Nov./Dec. 1998

[19] M. A. Masrur, Z. Chen, B. Zhang, and L. Murphey, "Model-based fault diagnosis in electric drive inverters using artificial neural network," *in Power Engineering Society General Meeting*, 2007. IEEE, 2006, pp. 1–7

[20] F. Zidani, D. Diallo, M. E. H. Benbouzid, and R. Naït-Saït, "A fuzzybased approach for the diagnosis of fault modes in a voltage-fed PWM inverter induction motor drive," *IEEE Transactions on Industrial Electronics*, vol. 55, no. 2, pp. 586-593, 2008.

[21] R. L. A. Ribeiro, C. B. Jacobina, E. R. C. Silva and A. M. N. Lima, "Fault detection of open-switch damage in voltage-fed PWM motor drive systems," *IEEE Transactions on Power Electronics*, vol. 18, no. 2, pp. 587–593, March, 2003.

[22] H. Fadil, Y. Driss, Y. Aite Driss, M.L. Larbi, and N. Abd Rahim, "Sliding-Mode Speed Control of PMSM with Fuzzy-Logic Chattering Minimization—Design and Implementation," *Information*, vol. 6, no. 3, pp. 432-442, Jul 2015.

[23] H. Fadil, L. Elhafyani, (In Press) "Fuzzy-PI Controller Applied to PMSM Speed Controller - Design and Experimental Evaluation," *Inter National Journal of Power ELECtronic*.

[24] D. Zhou, J. Zhao, and Y. Liu, "Predictive Torque Control Scheme For Three-Phase Four-Switch Inverter-Fed Induction Motor Drives With DC-link Voltages Offset Suppression," *IEEE Transaction on Power Electronics*, vol. 30, no. 6, pp. 3309-3318, Jun 2015

[25] T. Geyer, G. Papafotiou, and M. Morari, "Model Predictive Direct Torque Control-Part I: Concept, Algorithm, and Analysis," *IEEE Transaction on Industrial Electronics*, vol. 56, no.6, pp. 1894-1905, Jun 2009.

[26] H. Fadil, D. Yousfi, Y.A. Driss, and A.R. Nasrudin, "Synchronization Techniques benchmarking of grid fault modes in single-phase Systems," *in Proc. of the Renewable and Sustainable Energy Conference, Ouarzazat, Morocco*, October 2014.

[27] K.C. Chen, S. Salimin, S. A. Zulkifli, R. Aziz, "Single Phase Inverter System using Proportional Resonant Current Control, " *International Journal of Power Electronics and Drive System,* vol. 8, no. 4, pp. 1913 - 1918, December 2017.

[28] H. Fadil, Y. Driss, M.L. Larbi, and Y. Aite Driss, "Four-Switch Three-Phase PMSM Converter with Output Voltage Balance and DC-Link Voltage Offset Suppression," *Information*, vol. 8, no. 11, pp. 1-12, Jan 2017.